ORIGINAL ARTICLE

Simplified pushover-based seismic risk assessment methodology for existing infilled frame structures

Al Mouayed Bellah Nafeh[1] · Gerard J. O'Reilly[1]

© The Author(s), under exclusive licence to Springer Nature B.V. 2023

Abstract

The evaluation of seismic risk in structures requires information on both site hazard and structural vulnerability. Hazard can be quantified via probabilistic seismic hazard analysis, while seismic vulnerability can be quantified using structural analysis; the former is typically specified via predefined national hazard models, whereas the latter is more structure-specific and can be computationally expensive depending on the numerical modelling and analysis procedure complexity. As a compromise, various simplified seismic response evaluation methods have emerged and been implemented in assessment codes and guidelines (e.g., N2 method in Eurocode 8, SPO2IDA in FEMA P695). Furthermore, the seismic assessment and rehabilitation of existing structures have seen the introduction of risk classification guidelines. These are tools to primarily assist practitioners and decision-makers in understanding and managing seismic risk and the possible implications of different retrofitting schemes. Risk classification guidelines typically use loading-based quantities such as the seismic capacity-to-demand ratio. However, several drawbacks are associated with adopting loading-based quantities, namely the lack of uniformity of the actual seismic risk, expressed as a mean annual frequency of limit state exceedance. To address these drawbacks, this paper outlines a relatively simple pushover-based methodology for the direct evaluation of seismic risk (PB-Risk) for non-ductile infilled frame structures. The article describes a step-by-step framework for the simplified characterisation of hazard, vulnerability and subsequently seismic risk. It is quick and easy to implement within a practical and code-based setting and can be adopted within risk classification guidelines. The application of the proposed PB-Risk methodology is demonstrated via several case study applications, and its robustness in characterising seismic risk with respect to other simplified non-linear static formulations for infilled frame buildings is shown.

Keywords PBEE · Seismic risk · Assessment · Risk classification · Pushover

✉ Gerard J. O'Reilly
  gerard.oreilly@iusspavia.it

  Al Mouayed Bellah Nafeh
  mouayed.nafeh@iusspavia.it

[1] Centre for Training and Research on Reduction of Seismic Risk (ROSE Centre), Scuola Universitaria Superiore IUSS Pavia, Palazzo del Broletto, Piazza della Vittoria 15, 27100 Pavia, Italy

🍅 Springer

1 Introduction

The seismic risk assessment of reinforced concrete (RC) structures with masonry infills is an important issue in modern earthquake engineering. This is because infilled RC buildings represent a large percentage of the southern European built environment, particularly the Italian building stock (Crowley et al. 2020). Additionally, a significant portion of infilled RC buildings was constructed before the introduction of modern seismic guidelines (i.e., before the 1970s) and was typically designed to resist gravity loads only. Structural elements were characterised by inadequate seismic detailing and no consideration for ductile failure mechanisms [i.e., capacity-based design (Fardis 2018)] was given. Additionally, masonry infill panels were typically not considered in the design process and their effects on the structural system's response were generally neglected. However, past experimental (Zhai et al. 2016; Basha and Kaushik 2016; Bergami and Nuti 2015; Morandi et al. 2018), analytical (Dolšek and Fajfar 2008; Fardis and Calvi 1994) and field reconnaissance (Ioanna et al. 2012; Parisi et al. 2012) campaigns have highlighted the detrimental effect of infill panels on the global response and their consequent vulnerability to ground-shaking events.

Nowadays, seismic risk is generally expressed in terms of the mean annual frequency of exceedance (MAFE) and is the result of convolving both seismic hazard and vulnerability. The former requires a proper characterisation of the exceedance probability of a particular intensity measure (IM) level at a given site over a certain time period. The latter requires the assessment of seismic performance through the accurate quantification of the exceedance of known performance levels, or limit states (LS), in structures. This is typically expressed in terms of fragility curves obtained via extensive numerical analysis. To reduce the computational burden associated with such analysis, simplified tools and non-linear static procedures for assessing structures have been developed and have been included in seismic guidelines. These simplified approaches generally utilise empirical formulations to estimate the seismic demand and capacity directly. This includes the N2 Method (Fajfar and Gašperšič 1996) in Eurocode 8 (EC8) (Standard 2003), the capacity spectrum method (CSM) (Freeman 1998) in ATC 40 (1996), SPO2IDA (Vamvatsikos and Cornell 2006) in FEMA P-58 (2012), and the displacement coefficient method (DCM) in FEMA 356 (2000), for example.

The seismic risk assessment and rehabilitation of existing structures has witnessed the introduction of risk classification schemes or guidelines in some countries. These aim to assist practitioners and decision-makers in understanding seismic risk and the possible implications of different retrofitting schemes when looking to improve one's seismic resilience. They use loading-based quantities such as the seismic capacity-to-demand ratios, where the capacity can be estimated using any of the aforementioned non-linear static methods or through extensive numerical analyses. Notable examples include the "*Life Safety Index*" (SI-LS) of Sismabonus (Cosenza et al. 2018) in Italy or the "*Percentage New Building Standard*" (%NBS) (MBIE 2017) in New Zealand. Issues may arise when using loading-based quantities, such as the difference in reliability between ratings obtained through detailed or simplified inspections (Ferner 2018). However, the most pronounced disadvantage would be the lack of risk uniformity of loading-based quantities in characterising a particular building's risk rating, shown in Sect. 2.

A more suitable alternative would be to express seismic risk associated with distinct LSs in terms of their annual probability of exceedance, as discussed by Pinto and Franchin (2016). Pinto and Franchin (2016) infer that the seismic assessment of existing structures

and the subsequent evaluation of annual probabilities of LS exceedance should be carried out with reference to three methods of analysis: (1) incremental dynamic analyses on detailed numerical models; (2) incremental dynamic analyses on equivalent single-degree-of-freedom (SDOF) oscillators; or (3) non-linear static procedures. The first two options require performing numerical assessments to calculate seismic risk, which can be computationally expensive and require specific expertise. Alternatively, as part of method 3, practitioners and engineers could be provided with simple and robust tools to estimate seismic risk. It would facilitate communication to stakeholders and decision-makers to reduce seismic risk, offer ease of applicability, and, most importantly, overcome known limitations in existing approaches.

This paper first discusses the limitations of adopting loading-based quantities in risk-classification schemes. It then addresses these shortcomings by presenting a relatively simple pushover-based methodology for evaluating the seismic risk, denoted PB-Risk. It is developed here for infilled RC frame buildings specifically but its extension to other typologies is still expected to be valid. It builds on existing literature to give a straightforward approach that may be considered guideline-ready for near-future adoption. Its implementation is illustrated using case study examples and compared with other code-based formulations previously mentioned; this shows the proposed PB-Risk tool as a suitable candidate as a result of its accuracy, robustness, and simplicity.

2 Risk uniformity in conventional seismic classification schemes

One of the first issues regarding risk quantification and classification via code-based approaches is the lack of uniformity in the outputs. This has been documented in studies such as Iervolino et al. (2018) and Shahnazaryan and O'Reilly (2021), for example. A simple study is presented here to demonstrate the implications of adopting a risk classification scheme using loading-based quantities. Several code-compliant and non-compliant SDOF systems were generated to simulate modern and existing structures. They were modelled with a bilinear hysteretic response and fundamental period, T, ranging from 0.2 to 2 s. They were designed for two ductility classes described in EC8: medium and high, corresponding to behaviour factors for RC frames, q, of 3.90 and 5.85, respectively. The systems were designed for a soil class C site in L'Aquila, Italy, whose peak ground acceleration (PGA) is 0.26 g (INGV). The resulting elastic and design spectra according to EC8 are shown in Fig. 1a. The design spectral acceleration, $S_d(T)$, was identified from the design spectrum, and the design force was calculated as:

$$F_b = \zeta S_d(T) m^* \lambda \tag{1}$$

where m^* is the effective mass and λ accounts for the anticipated first mode response participation, taken here to be unity. Most importantly, a strength modification factor, ζ, was included to weaken the overall strength capacity of the SDOF systems and act as a proxy for non-code compliant structures. It ranged between 0.05 (i.e., weakest) and 1.0 (i.e., code-compliant) with an increment of 0.05. No additional overstrength was considered for the systems, although its inclusion is not anticipated to have an impact on the relative trends discussed later. A total of 360 SDOF oscillators were thus sampled (i.e., 2 ductility classes, 9 periods of vibration, 20 values of the strength modification factor). For each combination of ductility class (i.e., behaviour factor), period of vibration and strength modification factor, the SDOF oscillator yield displacement was then computed. The effect
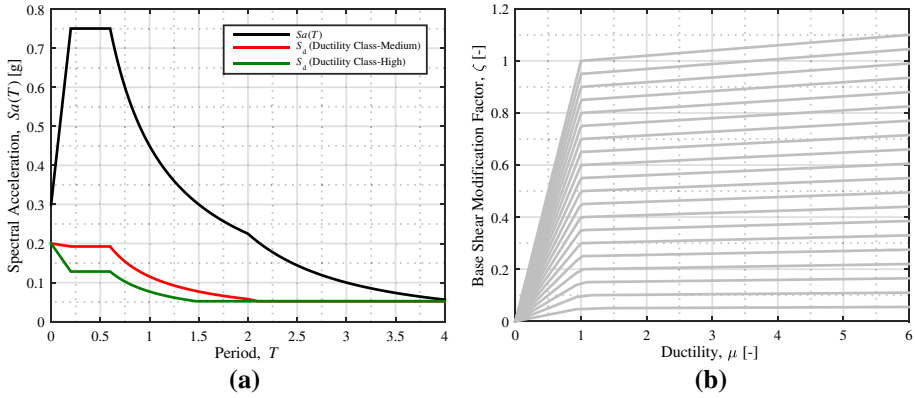
Fig. 1 **a** Elastic and design spectra from EC8 for a site in L'Aquila; **b** Example of SDOF oscillators ($T = 0.3$ s and $q = 3.90$) illustrating the degradation in lateral strength with respect to the code-compliant value for the design base shear
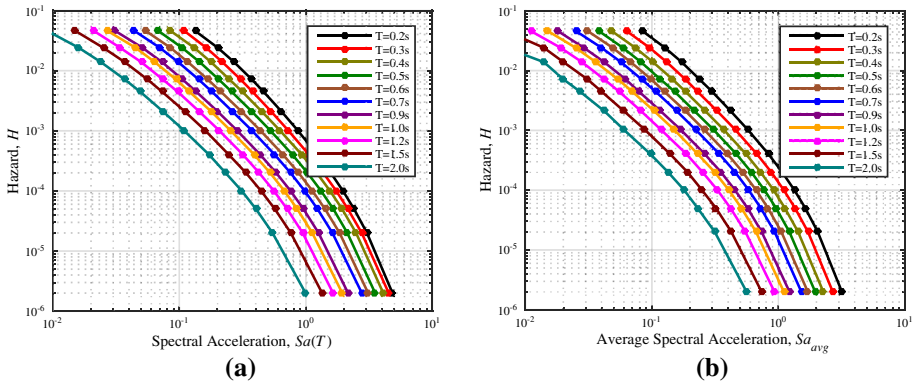
Fig. 2 Seismic hazard curves for the site in L'Aquila for **a** $Sa(T)$ and **b** Sa_{avg}

of ζ on the lateral response of the SDOF oscillators is illustrated in Fig. 1b for a subset of 20 SDOFs, expressed in terms of the base shear coefficient (i.e., design force normalised by total seismic weight) and ductility. Non-linear time-history analysis (NLTHA) using multiple stripe analysis (MSA) (Jalayer and Cornell 2009) was performed using hazard-consistent ground motion records to characterise the seismic response of the SDOF oscillators. The spectral acceleration at the fundamental period, Sa(T), was adopted as the IM. Hazard was characterised using the OpenQuake engine (Pagani et al. 2014) along with the 2013 Euro-Mediterranean seismic hazard model (ESHM13) (Woessner et al. 2015). The mean hazard curves are shown in Fig. 2a.

The seismic risk, defined as the mean annual of frequency of exceeding an LS threshold, λ_{LS}, was calculated by convoluting the results of hazard and fragility analyses from:
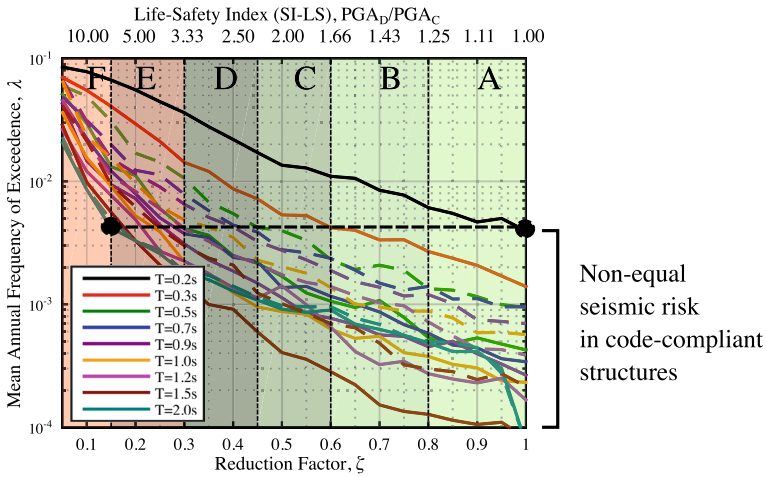
Fig. 3 Non-uniformity of risk for SDOFs for both medium (solid lines) and high (dashed lines) ductility classes versus periods of oscillation, T, and strength modification factor, ζ

Table 1 Sismabonus risk classification classes using PGA capacity-to-demand ratios only (Cosenza et al. 2018)

Life-safety index (SI-LS)	Building class	Life-safety risk description
$100\% \leq$ SI-LS	A+	Low (Code-compliant)
$80\% \leq$ SI-LS $< 100\%$	A	
$60\% \leq$ SI-LS $< 80\%$	B	Low to Medium
$45\% \leq$ SI-LS $< 60\%$	C	Medium
$30\% \leq$ SI-LS $< 45\%$	D	High
$15\% \leq$ SI-LS $< 30\%$	E	Very High
SI-LS $\leq 15\%$	F	

$$\lambda_{LS} = \int_{0}^{+\infty} P[\mu \geq \mu_{LS}|IM = s]|dH(s)| \tag{2}$$

where $P[\mu \geq \mu_{LS}|IM = s]$ corresponds to the conditional probability of exceeding an LS ductility capacity, μ_{LS}, and μ is the ductility demand at IM value s; $|dH(s)|$ is the absolute value of the hazard curve slope at the particular intensity, s. Considering this comparative case study application, the seismic risk was evaluated for a ductility of $\mu_{LS} = 4$.

The results, expressed in terms of λ_{LS}, are shown in Fig. 3. The seismic risk class of each SDOF oscillator was determined according to Sismabonus (Table 1), where A to F designate the risk classifications. These risk classes were determined based on the SI-LS index, defined as the ratio between the PGA demand at a return period of 475 years and the equivalent PGA capacity of the SDOF systems (i.e., PGA_D/PGA_C). Figure 3 illustrates the variability in the actual risk characterised via λ_{LS} versus T and ductility class. Additionally, the trends between λ_{LS} and ζ are demonstrated. Overall, it is evident that despite keeping the risk of LS failure at relatively low values (i.e., 10^{-3}–10^{-4}), seismic design implemented
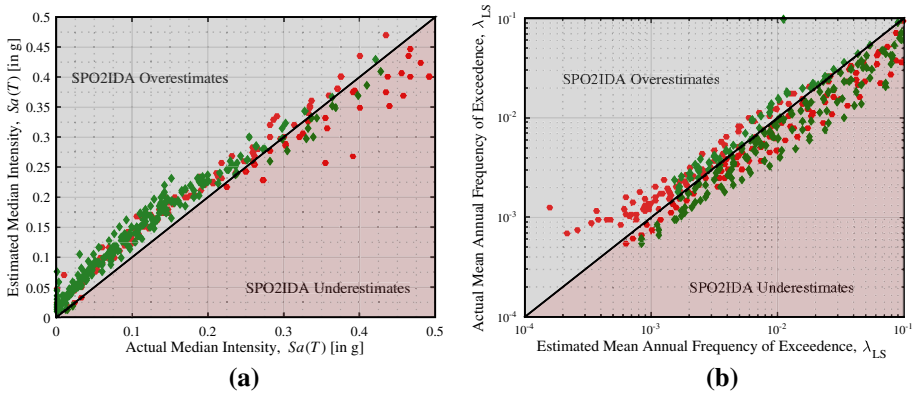
Fig. 4 Comparison of the median intensity and MAFE value estimated from SPO2IDA versus detailed analysis for both medium (green) and high (red) ductility classes

within EC8 does not result in uniform risk solutions. The shortcomings of this become more evident when assessing existing structures, where the capacity is generally not code-compliant (i.e., $\zeta < 1$). Belliss et al. (2016) also highlighted this for %NBS adopted in New Zealand. Figure 3 shows that many different risk classes can result for the same λ_{LS} depending on the period and ductility class. For example, following the horizontal line sketched in Fig. 3, a $T = 2.0$ s system with medium ductility class is classified F, whereas a $T = 0.2$ s system also with medium ductility class is classified A, despite the same level of actual risk. Furthermore, a vertical comparison in Fig. 3 highlights that code-compliant systems possess widely varying values of λ_{LS}. Overall, Fig. 3 gives and clear and straightforward illustration of the non-uniformity of current code-based design and assessment guidelines, which has also been observed by several studies in different contexts to date (Belliss et al. 2016; Li et al. 2010; Shi et al. 2012; Baltzopoulos et al. 2021; Gkimprixis et al. 2019; Ulrich et al. 2014; Douglas et al. 2013).

These observations emphasise that more effort should be made to express seismic risk via methodologies that better represent demand and capacity while still offering an acceptable trade-off between simplicity and accuracy. For example, SPO2IDA has been shown to be a suitable non-linear static procedure for characterising seismic response. It requires just the results of a static pushover analysis, and dynamic capacity of the structure is estimated empirically. Applying this tool to the same SDOFs just examined gives the results shown in Fig. 4, shown as the median intensity corresponding to $P[\mu \geq \mu_{LS} = 4|s]$ and the associated risk λ_{LS}. Compared to the outputs of extensive analysis previously described in Fig. 3, SPO2IDA shows quite a good agreement both in terms of median intensities and risk.

This case study application has two main conclusions: (1) loading-based quantities, such as the SI-LS index adopted by the Italian Sismabonus risk classification scheme, are not consistent in conveying risk estimates, despite their ease of applicability and compatibility with existing codes; and (2) simplified tools based on non-linear static analysis can offer a competitive solution with very low computational cost.

However, for the seismic response evaluation of non-ductile infilled RC frames, it was previously highlighted by Nafeh et al. (2020) that SPO2IDA is not an appropriate candidate. This is because the tool incorporates empirical relationships developed primarily for typologies such as newly-designed RC and steel moment-resisting frames,

which do not reflect the change in seismic behaviour due to non-ductile mechanisms and the addition of masonry infills. To remedy this, Nafeh and O'Reilly (2022) have recently proposed an unbiased seismic fragility estimation tool for this typology that also utilises just a static pushover analysis as its input. It also avoids issues of potential bias that may arise from a suboptimal IM choice. In the following sections, a methodology to evaluate the seismic risk for infilled RC typology using this tool is presented, along with an example application. Its accuracy is then compared to existing methods found in current codes and guidelines and the results from extensive NLTHA, particularly to calculate risk metrics to illustrate the added value.

3 Proposed methodology for simplified seismic risk evaluation

To address the lack of risk uniformity in loading-based quantities for evaluating and communicating seismic risk, a simple and efficient pushover-based method for the seismic risk evaluation (PB-Risk) explicitly tailored for non-ductile infilled RC frame structures is presented herein. The method utilises closed-form expressions to characterise the seismic hazard and integrates it with results obtained from the response evaluation tool developed for infilled RC frame buildings by Nafeh and O'Reilly (2022). This tool is based on intensive numerical analyses performed on equivalent SDOF models with a multi-linear force–displacement relationship representing infilled RC frame structures (Nafeh et al. 2020). It estimates the seismic demand using the response obtained from non-linear static analysis along with the first-mode parameters from eigenvalue analysis as inputs. Subsequently, the seismic intensity required to attain a particular limit-state of interest, expressed in terms of the average spectral acceleration, Sa_{avg}, can be identified. The tool (O'Reilly and Nafeh 2021a) has been implemented in a spreadsheet for ease of applicability and is available at: https://github.com/gerardjoreilly/Infilled-RC-Building-Response-Estimation. It possesses several improvements over existing response estimation methods available in the literature, such as reduction of bias, improved overall accuracy in the response estimation, amongst others. Interested readers are referred to Nafeh and O'Reilly (2022) for further details. Building from this, the PB-Risk methodology is illustrated in Fig. 5 and its details are described in the following sections along with an example demonstration in Sect. 3.4.

3.1 Hazard identification

Hazard analysis typically involves the characterisation of earthquake sources (i.e., faults, area sources) relative to a particular site, the frequency of occurrence and the identification of a relationship between earthquake characteristics and the intensity of ground-shaking. To do this, probabilistic seismic hazard analysis (PSHA) is performed, where the annual rate of exceeding a specified ground motion intensity level is identified. Open-source tools for conducting PSHA are available [e.g., OpenQuake (Pagani et al. 2014)]. Following PSHA, the mean hazard curve for a particular IM at a given site location is obtained. In the proposed method described for infilled RC frames herein, average spectral acceleration, Sa_{avg}, described by Eads et al. (2015) and adopted in many recent studies (O'Reilly 2021a,
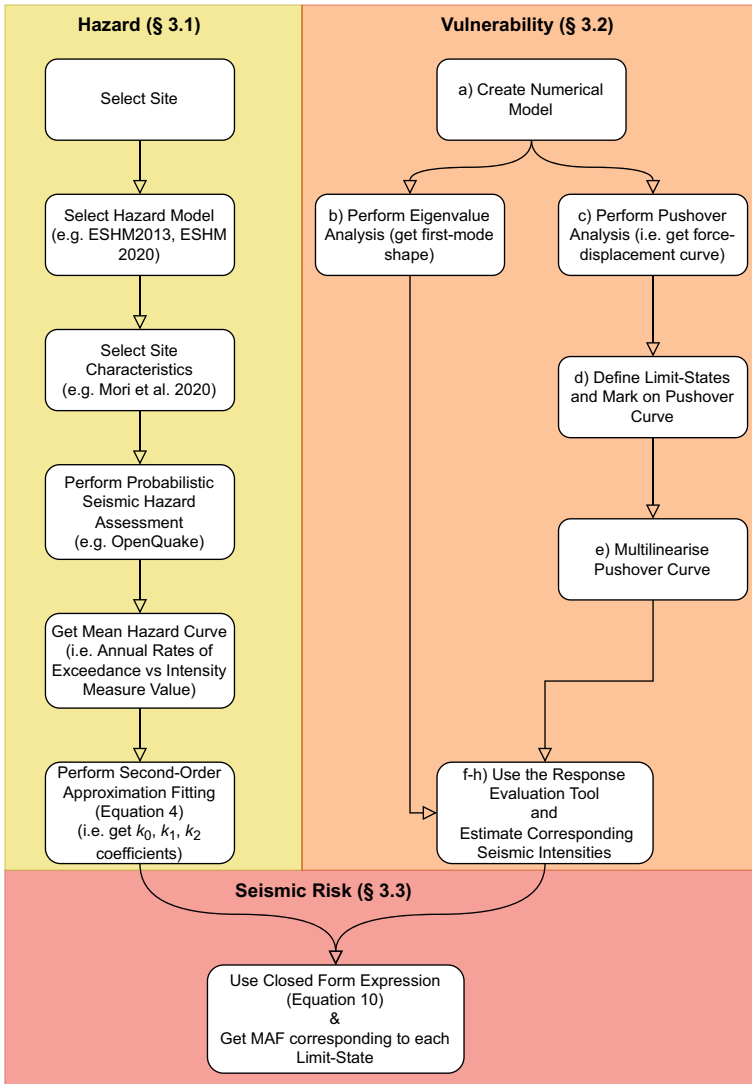
Fig. 5 Flowchart of the steps required for the proposed PB-Risk methodology

2021b; Qian and Dong 2020; Kohrangi et al. 2017) exhibiting promising results, is adopted as the IM. It is calculated as:

$$Sa_{avg} = \left(\prod_{i=1}^{N} Sa(c_i T) \right)^{1/N} \tag{3}$$

where c_i represent $N = 10$ number coefficients in the range of 0.2–3.0. The adoption of Sa_{avg} is due to the distinct advantages it offers in terms of increased efficiency and unbiased response estimation discussed by O'Reilly (2021b) compared to more conventional IMs

like $Sa(T_1)$ or PGA. Once the mean hazard curve is characterised, the second-order polynomial fitting function described by Vamvatsikos (2013) is used:

$$H(s) = k_0 \exp\left[-k_2 ln^2(s) - k_1 \ln(s)\right] \tag{4}$$

where $H(s)$ is the hazard function expressing the mean annual rates of exceeding an IM value s, and k_0, k_1 and k_2 are positive real numbers describing the hazard fitting coefficients. Adopting this second-order polynomial function for the hazard curve instead of simply integrated the actual hazard curve directly in Eq. 2 was preferred in order to provide simple and clear expressions whose coefficients are clearly traceable from one step to the next (Fig. 5). Although there may be some very minor price to be paid in terms of accuracy, it is not deemed significant based on the evaluations conducted by Vamvatsikos (2013).

3.2 Vulnerability estimation

Following the characterisation of seismic hazard at a particular site, the expected seismic response of the given structure under scrutiny is needed to assess its seismic vulnerability. This requires the response characterisation and the estimation of the seismic intensities corresponding to code-prescribed or other similar LSs. The steps required are as follows:

(a) Build a sufficiently detailed numerical model of the structure under consideration, or adopt a sufficiently accurate simplified method that accounts for all possible inelastic mechanisms and potential failure modes expected in the structure;

(b) Perform an eigenvalue analysis to extract the first-mode shape ordinates Φ_i and identify the seismic mass m_i at each floor level i. This mode shape is then normalised to the roof level's value (i.e. $\Phi_{roof} = 1$);

(c) Perform a non-linear static pushover analysis in both principal directions of the MDOF structure to obtain the base shear versus roof displacement data, F and Δ, respectively. To do this, a displacement-controlled inverse triangular pattern can be adopted for simplicity, in addition to first-mode based or an adaptive pushover procedure, depending on the complexity and particular characteristics of the structure;

(d) Fit a multi-linear backbone model to the MDOF's non-linear static pushover curves in both directions, which adequately captures the onset and end-point of each response
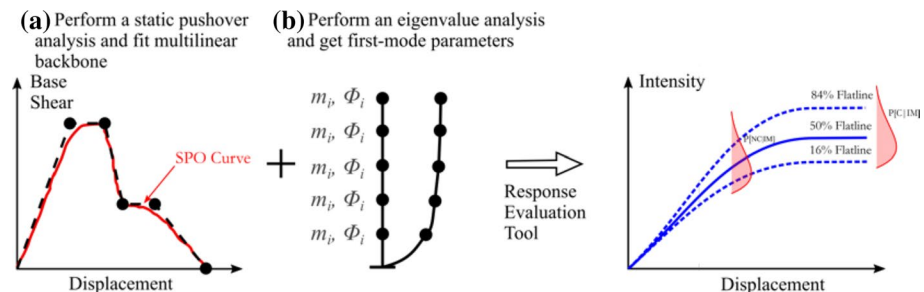

Fig. 6 Graphical illustration of the seismic response evaluation tool used for infilled RC frame structures

branch (i.e., elastic, hardening, softening, residual plateau and strength-degradation) as illustrated in Fig. 6 and further detailed in Nafeh and O'Reilly (2022);

(e) Identify the LS criteria to be checked from either code-based demand thresholds, or other ad-hoc definitions, and mark them on both pushover curves. These can be either local demand thresholds (e.g., yield rotation exceedance in a column member) or a global threshold (e.g., 0.5% storey drift);

(f) Using the response evaluation tool proposed by Nafeh and O'Reilly (2022) to estimate the unbiased seismic response capacity of the infilled RC system, the equivalent SDOF parameters based on a first-mode transformation factor, Γ, (i.e. $F^* = F/\Gamma$ and $\Delta^* = \Delta/\Gamma$) and the effective mass, m^*, are computed as per Eqs. (5)–(9), where T^* is the fundamental period of the equivalent SDOF oscillator; Sa_y^* is the yield spectral acceleration of the equivalent SDOF; F_y^* and Δ_y^* are the SDOF yield force and displacement values obtained by dividing the MDOF structure values by Γ, respectively. Each step is implemented automatically by the tool once the essential ingredients from the MDOF pushover and eigenvalue analysis in both directions are provided;

(g) Using the response evaluation tool, the seismic demand-intensity model is calculated for the structure's equivalent SDOF in both directions. It is expressed in terms of a dynamic strength ratio, $\rho = Sa_{avg}/Sa_y$, and global ductility, $\mu = \Delta/\Delta_y$. It estimates both the collapse and non-collapse performance of the equivalent SDOF structure. This means that for each LS previously identified, which has a corresponding μ, the median value of ρ required to exceed it is computed;

(h) Lastly, via the same tool, the median seismic intensities required to exceed both the non-collapse-based LSs and the overall collapse capacity of the structure, expressed in terms of Sa_{avg}, are computed for the actual MDOF structure through the reverse application of the equivalent SDOF transformation factor, as per Eq. (9).

$$m^* = \sum m_i \Phi_i \tag{5}$$

$$\Gamma = \frac{\sum m_i \Phi_i}{\sum m_i \Phi_i^2} \tag{6}$$

$$T^* = 2\pi \sqrt{m^* \frac{\Delta_y^*}{F_y^*}} \tag{7}$$

$$Sa_y^* = \frac{4\pi^2 \Delta_y^*}{T^{*2} g} = \frac{F_y^*}{m^* g} \tag{8}$$

$$\widehat{Sa}_{avg} = \rho Sa_y^* \Gamma \tag{9}$$

This then provides the median intensities in terms of the seismic intensity measure $\widehat{Sa}_{avg}$ for the set of LSs specified. For fragility analysis, a lognormal distribution was considered which is characterised by a median intensity and an associated dispersion. This dispersion can be due to various sources of uncertainty, such as record-to-record variability and modelling uncertainty, and are generally grouped as either aleatory or epistemic uncertainties. Nafeh and O'Reilly (2022) provide fixed values of dispersion for the non-collapse LSs,

β_{NC}, and the collapse LS, β_C, of 0.27 and 0.38, respectively. It is important to stress that these values represent record-to-record variability only and were determined using cloud analysis with Sa_{avg} as the IM. Other sources of uncertainty can be considered from other studies using suitable combination rules to amplify the dispersion values described here.

3.3 Seismic risk evaluation

Once the seismic hazard and vulnerability have been characterised, the seismic risk expressed in terms of the mean annual frequency of exceeding a pre-defined demand-based LS, λ_{LS}, can be calculated. To do this, the closed-form intensity-based formulation of the SAC/FEMA framework (Cornell et al. 2002) developed by Vamvatsikos (2013) is adopted and is described in Eq. (10):

$$\lambda_{LS} = \sqrt{p} k_0^{1-p} \left[H\left(\widehat{Sa}_{avg} \right) \right]^p \exp \left[\frac{k_1^2}{4k_2} (1 - p) \right] \tag{10}$$

$$p = \frac{1}{1 + 2k_2 \beta^2} \tag{11}$$

where β represents the dispersion and would correspond to β_{NC} or β_C for non-collapse and collapse LSs, respectively, if just record-to-record variability is considered whereas, $\widehat{Sa}_{avg}$ represents the median intensity measure required to attain a particular demand-based level. The corresponding value for $\widehat{Sa}_{avg}$ at each LS is obtained following the vulnerability estimation in Sect. 3.2. $H\left(s = \widehat{Sa}_{avg} \right)$ denotes the annual rate of exceedance for a given intensity s, defined following seismic hazard analysis in Sect. 3.1. This estimation of λ_{LS} for each LS represents its risk in terms of MAFE. As mentioned previously, while a direct integration of Eq. (2) would be ideal, this closed-form expression in Vamvatsikos (2013) can be carried out relatively easily rendering it simpler for practitioners and code-based applications.

3.4 Example application

To illustrate the PB-Risk implementation elements, an example corresponding to a 2-storey non-ductile infilled RC building with taxonomy code GLD-A-2st, previously defined in Nafeh et al. (2022) and taken from a database (O'Reilly and Nafeh 2021b) and located in Napoli, Italy, is presented. First, following the steps in Sect. 3.1 and illustrated in Fig. 5, PSHA was carried out using the OpenQuake engine to obtain the mean hazard curve and fit the second-order polynomial described in Eq. (4) and shown in Fig. 7, whose coefficients were found through a least-squares regression to be $k_0 = 1.42\mathrm{e}{-04}$, $k_1 = 3.50$ and $k_2 = 0.49$. The hazard analysis considered a fundamental period of $T = 0.2$ s and Sa_{avg} as the IM. The ESHM13 hazard model (Woessner et al. 2015) combined with the site characteristics using the mapping of the Italian territory presented by Mori et al. (2020) were used.

Second, following the steps in Sect. 3.2 and illustrated in Fig. 5, the structure was modelled in OpenSees using a three-dimensional lumped plasticity approach. The numerical model of the two-storey infilled RC building is shown in Fig. 8, and full details can be found in Nafeh and O'Reilly (2022). A non-linear static pushover analysis was performed
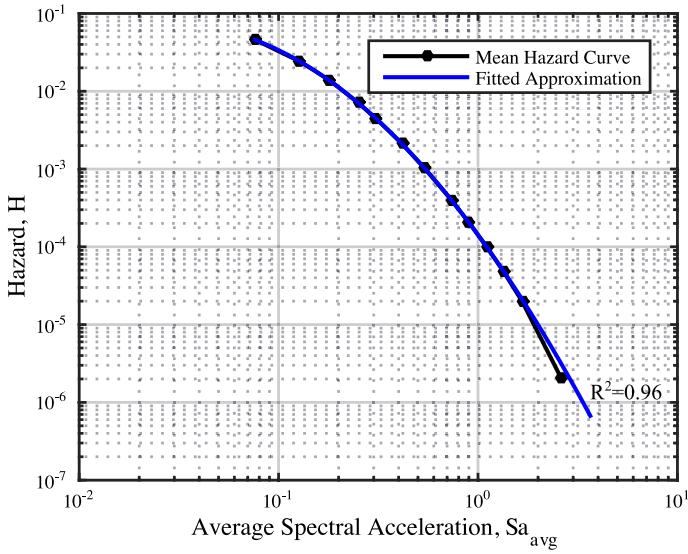
Fig. 7 Mean hazard curve and fitted second-order polynomial for a site in Napoli, Italy
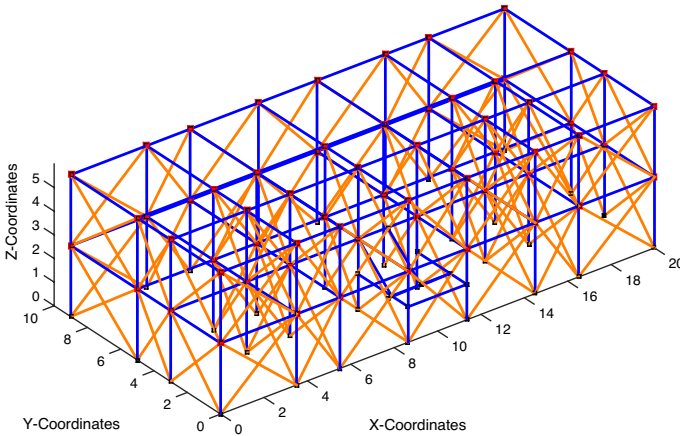

Fig. 8 Numerical model of the two-storey infilled RC building GLD-A-2st from (O'Reilly and Nafeh 2021b)

using an inverse-triangular and displacement-controlled lateral load pattern applied in both directions to obtain the base shear force versus roof displacement response, as shown in Fig. 9. In addition, an eigenvalue analysis was carried out to identify the first-mode shape ordinates, reported in Table 2. These correspond solely to the values of the first-mode shape ordinates and the seismic mass at each floor. The pushover curves were then fitted with a multi-linear fit to account for the various branches of the non-linear response of the infilled RC frame structure, as illustrated in Fig. 9. The equivalent SDOF oscillator
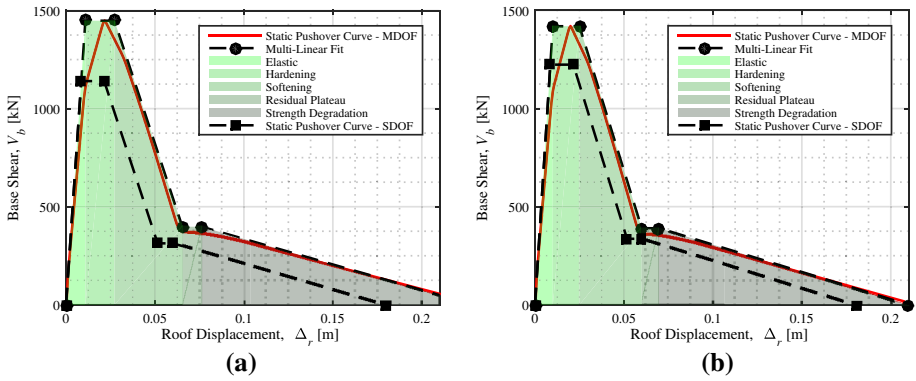
Fig. 9 Non-linear static pushover curves for the *X*-direction (**a**) and *Y*-direction (**b**) showing base shear and the roof displacement and the multi-linear fits to compute the equivalent SDOF properties

properties were then calculated following Eqs. (5)–(8) by applying the first-mode based transformation on the multi-linearised backbone curve of the MDOF system.

With the equivalent SDOF's backbone parameters defined, the seismic response for both non-collapse and collapse scenarios was then estimated using Nafeh and O'Reilly (2022). Equation 12 computes the median $\widehat{Sa}_{avg}$ intensity required to exceed a ductility-based LS in the MDOF system conditioned on no collapse. The resulting demand-intensity model for any ductility value is illustrated in Fig. 10a. This median and the noted dispersion value allow practitioners to quickly estimate the fragility functions for any ductility-based LS. These are shown in Fig. 10b for two LSs, which correspond to a roof displacement of 0.01 m and 0.025 m. This was an arbitrary definition made for the sake of illustration and other code-based LSs can also be handled, which is seen in Sect. 4.

$$\widehat{Sa}_{avg|NC,X,LS1} = \rho_{NC,X,LS1} \ Sa^*_{y,X} \ \Gamma_X = (0.71)(0.37g)(1.18) = 0.31g$$
$$\widehat{Sa}_{avg|NC,X,LS2} = \rho_{NC,X,LS2} \ Sa^*_{y,X} \ \Gamma_X = (1.05)(0.37g)(1.18) = 0.46g \qquad (12)$$
$$\beta_{NC} = 0.2$$

Equation 13, on the other hand, reports the equivalent expression to identify the median $\widehat{Sa}_{avg}$ intensity needed to result in collapse of the MDOF system. Again, this value along with the prescribed dispersion means the collapse fragility function for the structure is obtained, which is also shown in Fig. 10b.

$$\widehat{Sa}_{avg|C,X} = \rho_C \ Sa^*_{y,X} \ \Gamma_x = (1.72)(0.37g)(1.18) = 0.75 \ g$$
$$\widehat{Sa}_{avg|C,Y} = \rho_C \ Sa^*_{y,Y} \ \Gamma_y = (0.99)(0.63g)(1.16) = 0.72 \ g \qquad (13)$$
$$\beta_C = 0.3$$

Lastly, to estimate the seismic risk via the mean annual frequency of exceeding these LSs (i.e. LS1, LS2 and collapse), the fragility functions shown in Fig. 10b and the hazard curve shown in Fig. 7 were integrated via the closed-form expression in Eq. 10. For brevity, the calculation is only demonstrated for LS1 in the *Y*-direction in Eqs. (14)–(16); however, the remaining values associated with this example are summarised in Table 3.

Table 2 Eigenvalue analysis and the equivalent SDOF parameters in the two principal directions X and Y, where the latter values are denoted by the parentheses

Floor	Mass, m_i [tonnes]	First-mode Shape, Φ_i [−]	Effective mass, m^* [tonnes]	Transformation factor, Γ [−]	Period, T^* [s]	Yield spectral acceleration, Sa_y^* [g]
0 (base)	–	–	340.64 (338.49)	1.18 (1.16)	0.33 (0.24)	0.37 (0.63)
1	215 (215)	0.58 (0.57)				
2 (roof)	215 (215)	1.00 (1.00)				
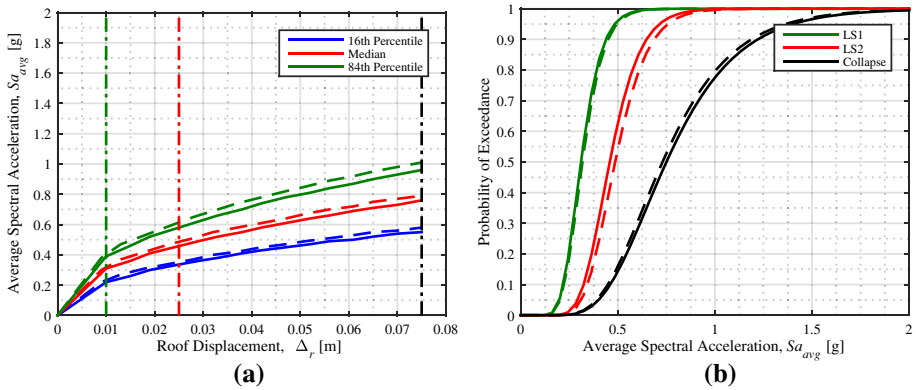
Fig. 10 a Demand-capacity curves obtained using the response evaluation tool, illustrating the median response and quantiles (16th, 84th) corresponding to the estimated average spectral acceleration intensity against the roof displacement of the MDOF system; **b** fragility curves corresponding to the two LSs. Solid and dashed lines denote the *X* and *Y* directions, respectively. Vertical lines correspond to the limit-state thresholds

Table 3 Summary of the simplified risk assessment results

Direction	Limit-state	$\widehat{Sa}_{avg}$	$H\left(\widehat{Sa}_{avg}\right)$	β	p	λ_{LS}	$T_R = 1/\lambda_{LS}$ [years]
X	LS1	0.31	0.0044	0.27	0.934	0.0051	195
	LS2	0.46	0.0016	0.27	0.934	0.0020	499
	Collapse	0.73	3.74e − 04	0.38	0.876	6.75e − 04	1481
Y	LS1	0.32	0.0044	0.27	0.934	0.0051	195
	LS2	0.49	0.0013	0.27	0.934	0.0017	498
	Collapse	0.75	3.91e − 04	0.38	0.876	7.01e − 04	1427

$$
\begin{aligned}
H\left(\widehat{Sa}_{avg}\right) &= k_0 \exp\left[-k_2 ln^2\left(\widehat{Sa}_{avg}\right) - k_1 \ln\left(\widehat{Sa}_{avg}\right)\right] \\
&= (1.42E - 04)\exp\left[-0.49 ln^2 0.31 - 3.50 \ln 0.31\right] = 0.0044
\end{aligned}
\tag{14}
$$

$$
p = \frac{1}{1 + 2k_2\beta_{NC}^2} = \frac{1}{1 + 2(0.49)\left(0.27^2\right)} = 0.93
\tag{15}
$$

$$
\begin{aligned}
\lambda_{LS1} &= \sqrt{p}k_0^{1-p}\left[H\left(\widehat{Sa}_{avg}\right)\right]^p \exp\left[\frac{k_1^2}{4k_2}(1-p)\right] \\
&= \sqrt{0.93}(1.42E - 04)^{1-0.93}[0.0044]^{0.93}\exp\left[\frac{3.50^2}{4(0.49)}(1 - 0.93)\right] = 0.0051
\end{aligned}
\tag{16}
$$

Additionally, the return periods, T_R, associated with the mean annual frequencies of each LS can be quantified, as shown in Table 3. This is particularly important for practitioners when carrying out a seismic performance assessment of an existing structure.

The code-based performance objectives can be checked depending on the code-based requirements. For example, if LS1 were checked at a risk level corresponding to a return period of 475 years, Table 3 shows that the return period is lower in both directions, meaning that the LS would not be verified.

4 Case study validation and comparison

Following its introduction for the seismic risk evaluation of infilled RC frame buildings in Sect. 3, a comparative assessment on a total of buildings was carried out to validate the robustness of the proposed PB-Risk methodology. To this end, a population of case-study buildings deemed representative of the infilled RC typology, typically found in Italy before the introduction of modern seismic design codes, was adopted. PSHA was performed to accurately characterise the hazard at a site of interest and allow the selection of hazard-consistent ground-motion records to perform extensive NLTHA analyses and accurately quantify the risk of exceeding several code-based LSs. Additionally, several existing methods used in various codes of practice and guidelines worldwide were investigated and comparatively assessed. These include the N2 method (Fajfar and Gašperšič 1996) with the consideration of inelastic spectra for infilled RC frames (Dolšek and Fajfar 2004), CSM (Freeman 1998), DCM (Federal Emergency Management Agency 2000) and the SPO2IDA (Vamvatsikos and Cornell 2006) tool to estimate the seismic response of the case study structures. These methods are non-linear static analysis methods for relatively fast quantification of seismic demand at a given return period intensity. For instance, using CSM, the level of expected structural displacement is quantified graphically based on the intersection of the capacity curve (i.e., the bilinearisation of the pushover curve) and the reduced or overdamped elastic spectrum. On the other hand, the N2 method uses strength and ductility relationships (i.e., R-μ-T relationships) to create an inelastic response spectrum that identifies the expected demand of the structure at a given return period. Furthermore, the DCM method is a relatively simple non-linear static procedure (NSP) used to determine the expected demand of the structure using a linear expression incorporating factors accounting for modal participation, maximum inelastic displacement to the linear elastic response, and the effect of the pinched hysteretic response type. Lastly, SPO2IDA relates the capacity of an MDOF system through non-linear static pushover curves to a set of interpolated IDA curves using empirical R-μ-T relationships based on a large dataset of SDOF structures. This case study comparison aims to assess the performance of the PB-Risk and existing methods in accurately quantifying the seismic risk associated with given LSs, λ_{LS}, in what may be seen as a modern PBEE-compliant manner (Günay and Mosalam 2013) for infilled frame structures.

4.1 Case-study buildings

A total of 40 non-ductile infilled RC case-study buildings with storeys varying from two to six were adopted from the same database of numerical building models (O'Reilly and Nafeh 2021b), accessible at: https://github.com/gerardjoreilly/Infilled-RC-Building-Database, for architectural layouts A, B, F and G. They were designed according to two approaches representative of Italian and the southern European construction practice,
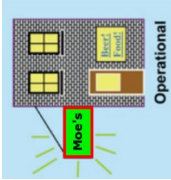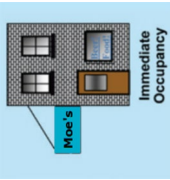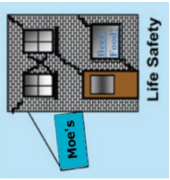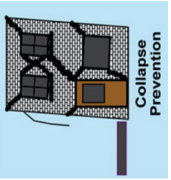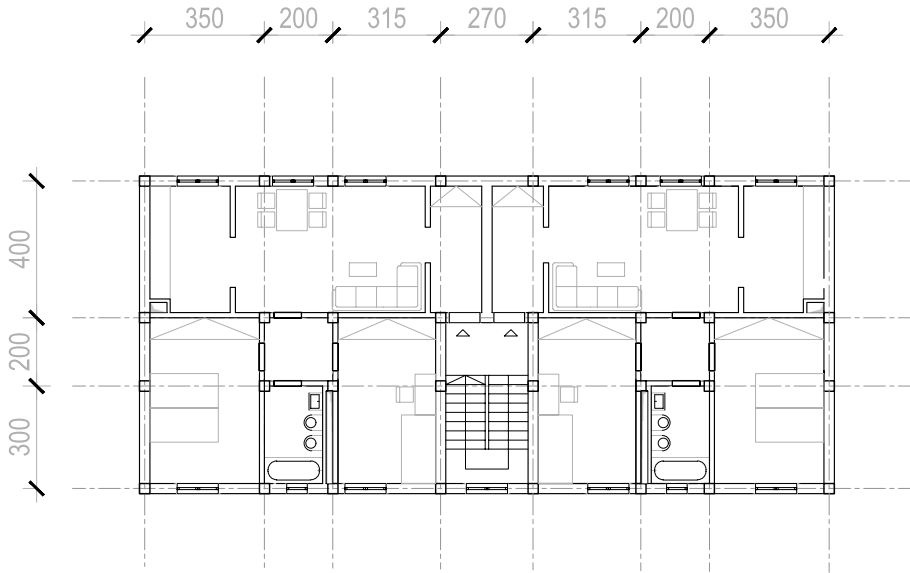
**Fig. 11** Plan layout of case study building A (2, 3, 4, 5 and 6 storeys)

namely: GLD (i.e., gravity-loads only, before the introduction of seismic provisions in the 1970s), and SSD (i.e., sub-standard design using the equivalent lateral force method, adopted between the 1970s and 1980s). Based on these characteristics, each building was labelled with an identification number used below: 2-A-GLD, for instance, denotes a two-storey building with architectural layout A and GLD provisions. For the sake of conciseness, only architectural plan layout A was illustrated as in Fig. 11. However, for further information regarding the database and the numerical modelling techniques employed, readers are referred to Nafeh and O'Reilly (2022).

4.2 Limit states and non-linear static pushover analysis

The first step in the case study application was identifying the code-based demand thresholds to be utilised and how they relate to the global pushover response. These demand-based thresholds described in the Italian national code (NTC2018) (Ministero delle Infrastrutture e dei Trasporti. D.M del 17 Gennaio 2018) were adopted for the comparative case study presented herein. A detailed description of the four adopted LSs is shown in Table 4. Additionally, these limit states are also dependant on the premature failure of the infill panels and the degradation in panel strength due to the in-plane-out-of-plane (IP-OOP) interaction (Milanesi et al. 2021; Morandi et al. 2022). However, this study focuses solely on the in-plane failure of the masonry panels. As such, the effect of the IP-OOP interaction was not considered. Following the definition of the NTC2018 LSs, non-linear static pushover analyses were conducted for each building in both principal directions. A displacement-controlled inverse triangular lateral load pattern was used for the SPO analyses, whose results are illustrated in Fig. 12. Then, the different performance points corresponding to each LS were identified on the SPO curves and are shown via markers in Fig. 12. It is worth recalling that the simplified analysis required for the vulnerability

Table 4 Description of the NTC2018 limit states and the associated damage observations

Limit-state	Description	Illustration
Stato Limite di Operatività 'Operational' (SLO)	Structural and non-structural elements maintain functionality without suffering damage and significant interruption of usage. Moderate damage to infill panels is foreseen at low levels of drift. The deformation capacity is equivalent to 2/3 of the deformation capacity at SLD	Operational
Stato Limite di Danno 'Damage Control' (SLD)	Structural and non-structural elements suffer moderate damage. Structure remains under immediate occupancy without jeopardizing human life. The overall capacity and stiffness of the structure is not compromised. The deformation capacity corresponds to the elastic limit of the bilinear equivalent model or reaching the yield chord rotation (θ_y) in a supporting column	Immediate Occupancy
Stato Limite di salvaguardia della Vita 'Life Safety' (SLV)	Structure sustains heavy damage to its structural elements resulting in a significant loss of lateral stiffness. The structure retains its gravity load carrying capacity with a margin of safety against collapse. Failure of non-structural elements is a direct consequence of attaining SLV. The ultimate displacement at SLV is defined as ¾ of the roof displacement at SLC or achieving 75% of the ultimate chord rotation (θ_u) in any component	Life Safety
Stato Limite di prevenzione del Collasso 'Collapse Prevention' (SLC)	Structural and non-structural elements suffer heavy damage. The structure maintains gravity-load carrying capacity with a slender margin of safety against collapse due to the full exploitation of the strength and deformation capacity. The SLC limit-state is defined as the point on the bilinear capacity curve where a residual capacity of 80% of the maximum base shear is achieved or the ultimate chord rotation (θ_u) is reached corresponding to any component	Collapse Prevention
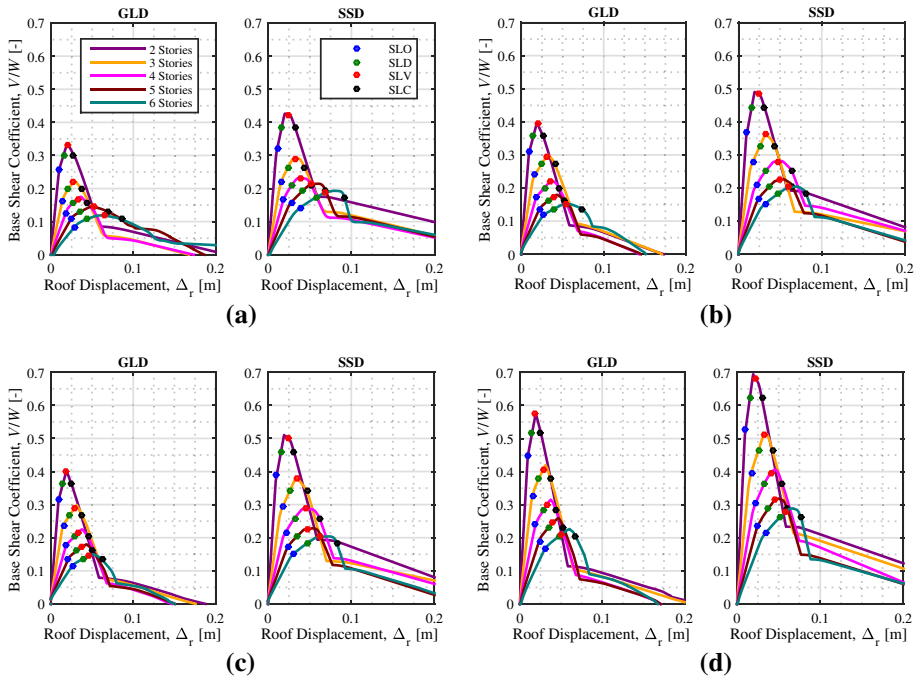
Fig. 12 Non-linear static pushover analysis curves for case study buildings with taxonomy codes **a** *-A-#; **b** *-B-#; **c** *-F-#; **d** *-G-#, where * denotes the design approach (i.e., GLD or SSD) and # denotes the number of storeys (i.e., 2, 3, 4, 5, 6)

assessment of existing structures using the response estimation tool should be carried out in the two principal directions. Then, the fragility results of the more critical direction at each limit-state should be considered. A single seismic risk value for each limit state can be identified. However, for brevity and clarity, only the results of the weaker directions are demonstrated here.

4.3 Seismic hazard and ground motion record selection

The case-study buildings were located in the central Italian town of L'Aquila, and PSHA was carried out using the OpenQuake engine (Pagani et al. 2014) considering $Sa(T_1)$ and Sa_{avg} as IMs. The inclusion of $Sa(T_1)$ was necessary to estimate risk via existing assessment methods. The mean hazard curves extracted from PSHA have been illustrated for both IMs in Fig. 2, and the second-order polynomial described in Sect. 3.1 and Eq. (4) was fitted. A suite of 25 records was then selected using the toolbox for ground motion selection and processing (EzGM) developed by Ozsarac et al. (2021). This was carried out at nine intensity levels corresponding to return periods of 22, 42, 72, 140, 224, 475, 975, 2475 and 4975 years to allow the characterisation of the structural response from initial damage of the masonry infill panels up to global structural collapse.

4.4 Extensive analysis and LS exceedance

MSA (Jalayer and Cornell 2009) was carried out to accurately characterise the non-linear dynamic response of the case study buildings at discrete intensity measure levels. This is a standard analysis procedure that uses the conditional spectrum (Baker 2011) to select ground-motion record sets consistent with the site hazard at each intensity level. This is as the causative parameters of the ground motion records generally change with increasing intensity level (Bradley 2010; Iervolino et al. 2010; Lin et al. 2013). For the derivation of fragility functions corresponding to LS exceedances using MSA, the analysis results obtained from non-linear response history analysis, expressed in terms of an engineering demand parameter value at each IM level, are obtained. The MSA results are then coupled with the maximum likelihood method (Baker 2015) to estimate the median intensity corresponding to LS exceedance, $\widehat{Sa_{avg}}$, and its associated dispersion, β, typically expressed via a lognormal distribution.

4.5 Simplified analysis and LS exceedance

As mentioned previously, the goal of this case study was to assess several structures using simplified methods and compare them with the results of more extensive dynamic analyses. The first comparison in this regard was to evaluate each method's ability to predict the median seismic intensity level associated with the exceedance of each LS described in Table 4. Results for existing practice-based methods (i.e., N2 method, CSM, DCM and the SPO2IDA tool) were expressed in terms of $Sa(T_1)$, while the outcome of the proposed PB-Risk methodology was defined in terms of Sa_{avg}. The results are shown in Fig. 13. Additionally, the application of the aforementioned NSPs (i.e., CSM, DCM, N2) was carried out following a code-based approach. This entails the use of code-based spectra solely without any further extension that may be available in recent literature [e.g., cloud-based capacity spectrum method (Nettis et al. 2021)], and without the need for real ground-motion-derived spectra. This complements the aim of the study where the proposed response evaluation tool is compared to other practice-based NSPs from a practical standpoint with reference to code-based applications. By no longer referring to ground-motions and NLTHAs, the computational burden can be significantly reduced since just a pushover analysis is required, rendering the proposed tool a practical alternative to other code-based NSPs, particularly for the case of non-ductile infilled RC structures.

Before delving into the comparative discussion of the results, some of the limitations of NSPs when compared to NLTHA are worth mentioning. A common feature of the NSPs examined here is their characterisation of the structure's response via static pushover analysis. It should be recalled that pushover analysis offers many advantages over detailed NLTHA, but also possesses some limitations when used as part of NSPs to characterise LS performance. These include its ability to capture the complex dynamic behaviour of MDOF systems where the first mode is not dominant, or situations where stiffness and strength degradation and other effects such as hysteretic pinching are notable. Another shortcoming is its difficulties capturing the impact of torsional behaviour in three-dimensional building models, although not observed here, although these can be addressed with some further consideration (Kaatsiz and Alici 2017; Kan and Chopra 1977; Fajfar et al. 2005). Thankfully, these aspects do not prevent NSPs from being used in practice but are worth recalling here as simplifying assumptions to be aware of. The limitations mentioned
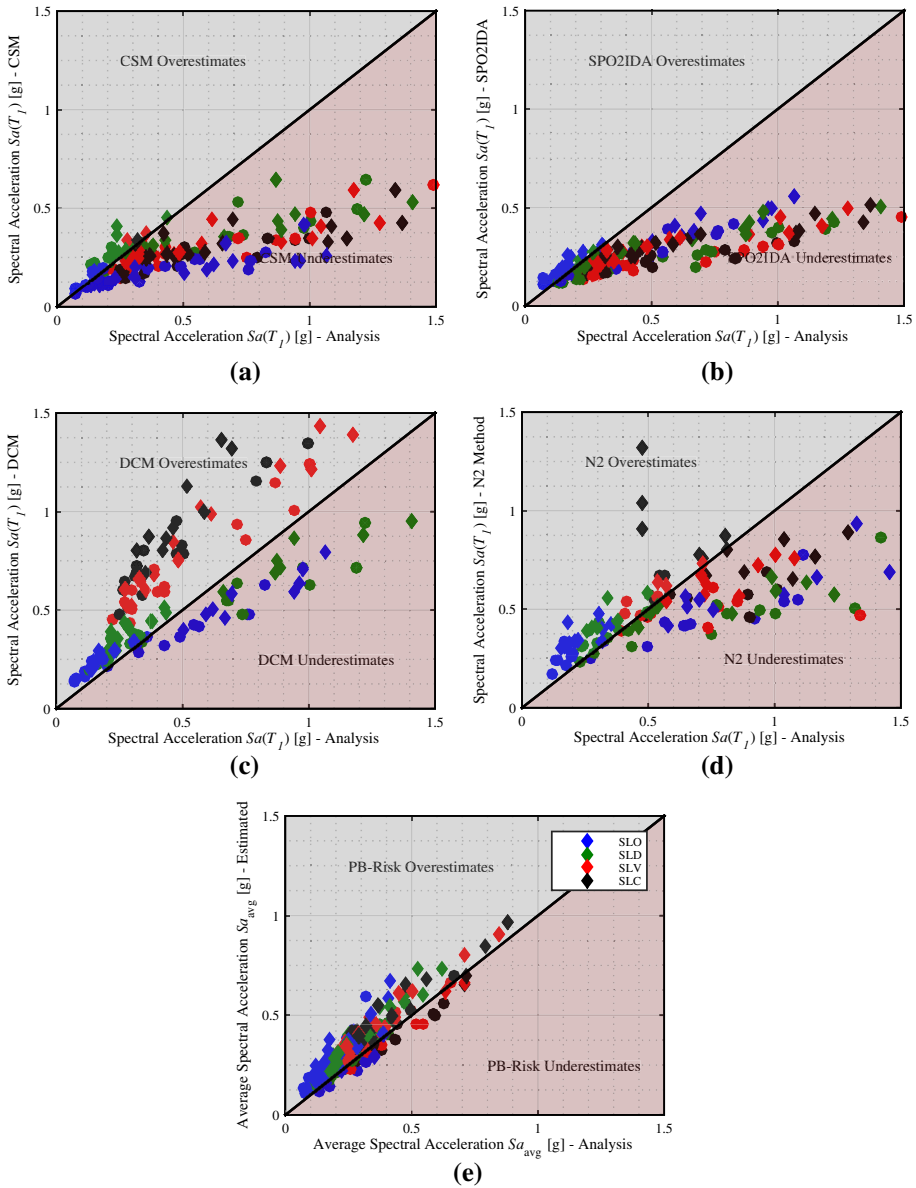
Fig. 13 Comparison of the different simplified methods when estimating the seismic intensity required to exceed the code-based limit states

were not deemed pertinent issues for the present case study comparison but are nonetheless noted as possible sources of error with respect to dynamic analysis results.

CSM was carried out referring to the ATC guidelines (1996) where an iterative procedure was outlined. Additionally, the elastic code-based spectrum employed in the N2 method (described below) was used and reduced using an equivalent viscous damping model until an intersection between the capacity curve and the reduced spectrum was

achieved. Inspecting Fig. 13a, it can be seen that the CSM has underestimated the median intensities with respect to the detailed NLTHA. This was an expected outcome of the CSM for the particular typology under scrutiny. Generally speaking, a significant drawback of the CSM is how it simply relates the hysteretic energy dissipation of an inelastic system with an equivalent viscous damping in an equivalent linear system, especially for highly inelastic systems (Krawinkler 1994). As demonstrated by Chopra and Goel (Baker 2015), other shortcomings are the non-convergence and underestimation of the actual seismic demand. Moreover, the traditional equivalent viscous damping model adopted for the CSM was developed mainly for bare RC frame structures. For the case of infilled RC frame structures, a higher viscous damping value is expected due to the additional energy dissipation of the masonry infill panels. This essentially renders the standard damping model invalid for the performance assessment of infilled structures. Since the equivalent viscous damping for infilled frames is expected to be higher than that of its bare RC counterpart, its impact becomes directly observable in the estimated seismic intensities. Because of the higher damping in the infilled system, a higher intensity is required to achieve a particular LS demand threshold compared to a bare RC frame. This is essentially the reason for the consistent underestimation of the CSM in Fig. 13a. Landi et al. (Landi et al. 2016) proposed an equivalent viscous damping model for infilled RC frame structures for displacement-based assessment applications. However, O'Reilly (2016) has illustrated that these expressions tend to significantly overestimate values associated with the EVD in comparison with actual NLTHA and also with experimental findings reported by Morandi et al. (Morandi et al. 2014), especially at low ductility levels despite the fact these estimates are improved for higher ductile levels of response where a limited ground motion set was used. Further work was noted to be required by Landi et al. (2016) in order to develop a more generalised formulation such as that proposed in Priestley et al. (2007) for ductile RC frames, for example. Hence, the EVD model proposed by Landi et al. (2016) was not adopted within this study and a comparative assessment using the conventional CSM was described instead. However, in its current form, it is clear that the original CSM approach is unsuitable for estimating LS fragility functions in infilled frame typologies.

Examining the comparison for SPO2IDA Fig. 13b, it is clear that the median intensities were not well represented for infilled RC frame structures, with a consistent underestimation of the median intensities. This is contrary to the observations previously made in Fig. 4 and like the CSM, it is again due to the fundamental difference in the behaviour of the framed structures. For systems modelled without masonry infills, the first mode dominates the response and a simple bilinear hysteretic model sufficiently captures the structural behaviour until collapse, as highlighted by Vamvatsikos and Cornell (2005). In the case of the infilled frame buildings, however, the addition of infills modifies the overall hysteretic behaviour from that of a bilinear system and increases its inherent energy dissipation capacity. This premature exhaustion of the masonry infill capacity at one or more storeys results in a fundamental change in response to cause a period shift and a modification of the first mode behaviour. Coupling this with the additional energy dissipation capacity of the infills means that the simplified method that does not account for their contribution would be expected to underestimate the median seismic intensities, as shown in Fig. 13b.

Examining the DCM in Fig. 13c, a large scatter in the median intensities was observed. A considerable overestimation of the median intensities required to exceed the higher LSs (i.e., SLV and SLC) can be observed where significant non-linear behaviour is expected. For the other LSs closer to elastic and slightly non-linear behaviour, the comparison appears to be more reasonable but still with a degree of scattering. These differences are because the DCM relies on several coefficients to account for the general characteristics of

the structural typology but not necessarily the specific structural behaviour. Coefficients are determined for the expected displacement (elastic and inelastic) ratio for a bilinear SDOF system, the effects of the pinching in-load deformation relationships due to stiffness and strength degradation, and second-order geometric non-linearities (i.e., *P-Δ* effects). These DCM coefficients were primarily calibrated for SDOFs with non-evolutionary hysteretic relationships, which was also described by Baltzopoulous et al. (2015) as a shortcoming to be addressed via the direct evaluation of the inelastic displacement ratios for degrading SDOF systems (Chenouda and Ayoub 2008). Moreover, the FEMA guidelines highlight potential errors associated with the utilised coefficients for systems with a fundamental period lower than 0.4 s, corresponding to many of the structures examined in Fig. 13c whose first mode periods range between 0.2 and 0.6 s.

The comparisons discussed so far have been for methods not directly tailored to account for infilled frame behaviour. Figure 13d and e, however, illustrate the comparisons for two methods directly intended for such application: the N2 method and the proposed PB-Risk methodology, respectively. For the code-based spectra, corner period values, corresponding to $T_B = 0.2$ s, $T_C = 0.6$ s, and $T_D = 2$ s were considered. This is similar to the recommendations of the NTC for building the elastic response spectrum considering a given value of PGA (0.26 g) and soil class C for the site of L'Aquila. Examining these plots, it is seen in Fig. 13e how the response estimation tool developed by Nafeh and O'Reilly (2022) utilised as a part of the proposed methodology offers a very good match with relatively low scatter at all LSs when compared to the detailed NLTHA. Similar results can also be seen for the N2 method in Fig. 13d, highlighting how the infill panels' direct consideration is vital to accurately quantify the seismic fragility of this building typology. Examining the results further shows that the N2 method underestimated the intensities required for several LSs at higher intensities. This may be due to the limitations in the *R-μ-T* relationships developed by Dolšek and Fajfar (2004), examined in Nafeh et al. (2020). For example, Miranda and Bertero (1994) noted that the strength reduction factor, *R*, used in the N2 method is generally more stable around the medium-to-long period ranges. Additionally, for short-period structures, such as infilled RC frame structures, inelastic deformations are larger than the elastic ones and thus the equal displacement rule adopted in the N2 method becomes no longer valid. This conclusion was noted among other limitations by Fajfar (2000). Other possible sources of this trend at higher intensities may be in the choice of IM. The tool proposed by Nafeh and O'Reilly (2022) utilises average spectral acceleration Sa_{avg} as its IM, whereas the N2 method is based on $Sa(T_1)$. O'Reilly (2021b) has investigated this comparison and highlighted some notable advantages of Sa_{avg} and several limitations of $Sa(T_1)$ when assessing these building typologies. Perhaps a promising alternative to the conventional code-based capacity spectrum and N2 methods examined in this study are the cloud-based CSM and N2 developed by Gentile and Galasso (2021) and Nettis et al. (2021). These introduce improvements to the existing well-known NSP through the application of real (i.e., recorded) ground motions. This is carried out to replace the adoption of code-based spectra to estimate the seismic intensities required to exceed code-based performance points and to explicitly account for the associated record-to-record variability in fragility analysis. Such improvements may help remedy the drawbacks of CSM and N2 method or in this case, explain the differences observed in Fig. 13a and d when applied to infilled structures. For example, according to Nettis et al. (2021), cloud-based CSM provided comparably accurate estimates with respect to the N2 method and classical non-linear time-history procedures for short and medium period cases such as infilled RC frame structures. In addition, Gentile and Galasso (2021) noted that non-linear dynamic analysis of SDOF systems is not substantially superior with respect to a non-linear static analysis

coupled with the capacity spectrum method for the case studies analysed. This observation may be further explored for the context presented here. One principal difference would be in how to account for the use of Sa_{avg} advocated here and shown to be notable advantageous (O'Reilly 2021b) versus the use of $Sa(T_1)$ in CSM, although this is not an unsurmountable issue.

In summary, the most notable improvements which were implemented in the development of the proposed PB-Risk methodology are: the adequate characterisation of the structural response using representative infilled RC SDOF oscillators considering the modelling approach suggested by Nafeh et al. (2020) which were considered for the development of the response estimation tool (Nafeh and O'Reilly 2022); the reduction of bias influencing the structural response due to the scaling of ground-motion records with the adoption of cloud analysis as a suitable dynamic method for the characterisation of empirical R-μ-T relationships; the reduction in the record-to-record variability following the consideration of Sa_{avg} as IM.

4.6 Evaluation of seismic risk estimation

Following the application of the PB-Risk and existing simplified pushover-based methods to estimate the median intensities for LS exceedance, this evaluation was further extended to the estimation of the MAFE of these LSs, λ_{LS}. As described in Sect. 3.3, seismic risk in single structures can be computed by convoluting seismic vulnerability and hazard at the site location via Eq. (10). As such, the median intensities (Fig. 13) were integrated with the corresponding hazard curves shown in Fig. 2. In the case of the PB-Risk method, the expected dispersion β was provided directly by the response evaluation tool; however, in the case of the other methods, dispersion values needed to be assumed in some cases. As previously discussed, the N2 and CSM methods were presented as code-based non-linear static procedures. This means that the code spectra were utilised for the assessment with no reference to a ground-motion set or NLTHA output. Hence, the assumption or estimation of a dispersion (associated with a median seismic intensity computed from N2 or CSM) corresponding to a particular demand-based threshold was necessary. For example, the dispersion from SPO2IDA was obtained from the IDA fractiles generated by the tool. The dispersion from the N2 method was estimated based on the recommended value of 0.7 for the coefficient of variation by Dolšek and Fajfar (2004). However, the dispersions associated with the CSM and DCM methods are not explicitly provided in these methods, nor is any indicative value suggested. A value of 0.25, 0.30, 0.35 and 0.40 were thus adopted for the SLO, SLD, SLV and SLV LSs, respectively based on the recommendations in O'Reilly (2016).

From this, the MAFE of each LS in the case study buildings were computed and are illustrated in Fig. 14. These results are expressed in terms of an MAFE ratio, $\lambda_{simplified}/\lambda_{extensive}$ where the $\lambda_{simplified}$ values were obtained using the simplified methods previously discussed and $\lambda_{extensive}$ refers to the NLTHA-based results. These were taken as the benchmark value as they involve extensive evaluation using MSA on detailed numerical models with suites of hazard-consistent ground motion records. The MAFE ratios shown in Fig. 14 were also grouped based on the number of storeys to illustrate any possible trends in this regard.

Figure 14a illustrates the MAFE ratios associated with the operational LS (i.e., SLO). The results show a reasonably good match of the seismic risk estimates using the considered NSPs compared to the extensive results. This observation was expected
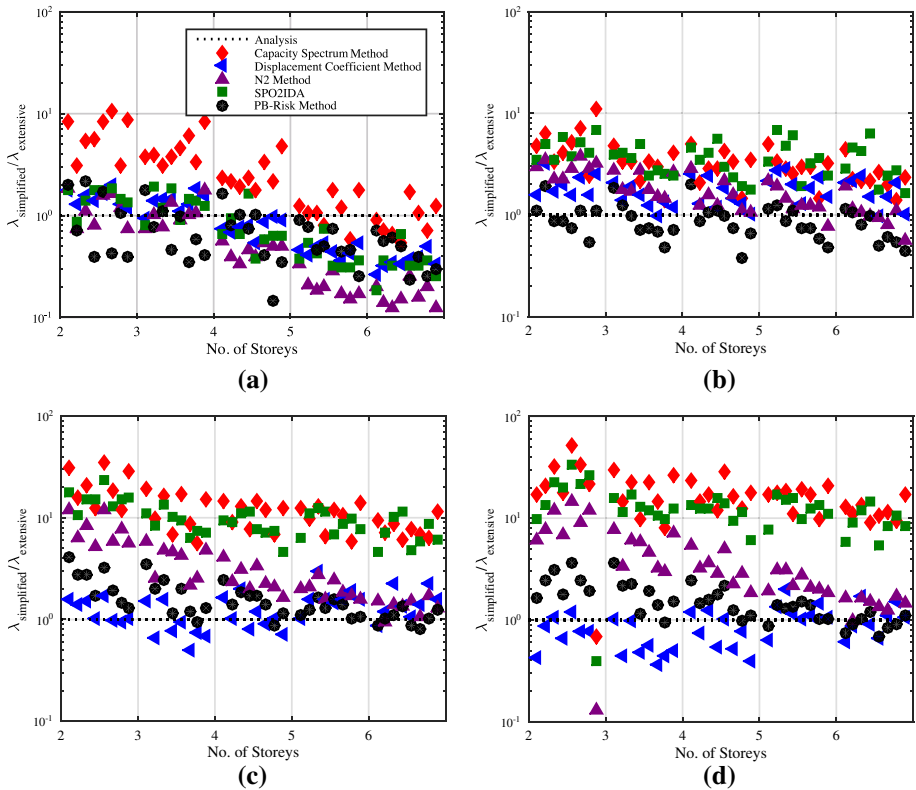
Fig. 14 Mean annual rate of exceeding the demand-based threshold associated with each of the NTC2018 limit states (i.e., SLO, SLD, SLV, SLC) and accounting for the seismic demand quantification using different practice-based methods and the proposed PB-Risk methodology

considering that all NSPs performed relatively well in estimating the median seismic intensities shown in Fig. 13 corresponding to an LS in the elastic range of response with relatively low dispersion. For the case of the CSM, a consistent overestimation of the seismic risk was observed due to the method's inability to adequately represent the seismic intensities required to achieve the SLO limit-state, leading to the underestimation observed in Fig. 13. The difference in risk estimates becomes more evident for LSs where inelastic behaviour is more prevalent. This can be observed in Fig. 14b–d, where methods such as SPO2IDA, CSM and DCM consistently overestimated seismic risk for all identified LSs. This again reflects the results of the previous section and indicates the conservativeness of those methods. For example, these methods overestimated the seismic risk by 2–8 times the benchmark value for the SLD limit-state. This overestimation increases to about 10–50 times the benchmark seismic risk value computed from extensive analysis for the SLV and SLC limit states.

This overestimation of λ_{LS} is the direct consequence of underestimating the seismic intensity associated with the four defined LS. Among the practice-based methods reviewed, the best performance was shown by the N2 method, which is a testimony to being the standard European practice for quantifying seismic demand and its inclusion in the EC8 standards. More importantly, regarding the proposed PB-Risk, a promising

performance was observed via the consistent estimation across the entire range of seismic response. Reasonable underestimation of risk was recorded for the operational limit-state (SLO), and more accurate estimations were observed for SLD, SLV and SLC. This is due to the tool's consistency in estimating the seismic demand associated with the four LS, as illustrated in Fig. 13e.

Considering this comparison and the evaluation of the seismic response in the previous section, it can therefore be noted that the proposed methodology can replicate the results obtained using extensive NLTHA while cutting down on computational time and effort without any compromise on the risk-based metrics.

5 Discussion

Performance-based earthquake engineering (PBEE) is now a well-known and established approach that allows users to evaluate a building's seismic performance from a probabilistic perspective. To do this, there is still scope for simple probabilistic-based alternatives to current practice that rely on a loading-based capacity-to-demand ratio. This was highlighted earlier in Sect. 2, where the implications of adopting deterministic quantities such as the SI-LS index were highlighted. It was also shown that loading-based quantities were inconsistent in communicating risk estimates and do not infer much, despite their simplicity, regarding the actual level of structural safety and the mean annual rate of exceedance of a given LS remains largely unknown. The use of probabilistic methods is an aspect that ought to be addressed in guidelines to evaluate seismic risk in existing buildings. In a leap forward, the second generation of EC8 and the Italian guidelines for the probabilistic assessment of seismic safety of existing buildings defined by the CNR (CNR 2014) have foreseen the introduction of standards which aim at filling this gap. They incorporate issues associated with multiple sources of uncertainty, such as the definition of limit states and target performances, probabilistic quantification of seismic action, knowledge acquisition and uncertainty modelling, structural analysis, identification of LS exceedance and assessment methodologies. In this regard, the methodology proposed here for infilled frames and described in Sect. 3 is compliant with the recommendations of these recent guidelines. This is especially the case regarding two main aspects related to performance: the quantification of seismic intensities for LS exceedance using the proposed non-linear static procedure for infilled RC buildings and in terms of the calculation of the required safety level expressed in terms of the MAFE.

Furthermore, these guidelines (CNR 2014) infer that a probabilistic framework should be carried out with reference to three analysis methods, depending on the level of complexity of the examined structure. The use of NSPs has proved robust for the structures discussed previously, offering a satisfactory trade-off between accuracy and computational burden. This was also noted in other studies, particularly on a regional scale performed on seismic prioritisation and screening of building portfolios. Such frameworks can either rely on easy-to-retrieve data based on nominal structural performance such as NODE (Petruzzelli and Iervolino 2021). Other studies have elected to develop relatively fast frameworks which also utilise low-level information and seek to estimate demand parameters (e.g., storey drifts, peak floor accelerations), such as STICK-IT (Gaetani d'Aragona et al. 2020), which can then be integrated with seismic prioritisation frameworks to be applied within large-scale assessment studies on seismic risk and associated losses. The proposed PB-Risk

methodology is still in line and compatible with these general approaches and could serve as a means to provide more refined performance quantification based on pushover analysis.

Overall, a simple pushover-based methodology for evaluating mean annual rates of LS exceedance for infilled RC frame structures was introduced for risk-based application. The method is relatively fast and straightforward as it relies on closed-form approximations to characterise hazard, vulnerability and subsequently the associated risk in single structures. Additionally, robustness, accuracy and consistency were highlighted despite the inherent simplicity of the method and the improvement offered compared to other NSPs. This is particularly the case for the infilled RC typology, whose limitations when analysed with conventional approaches not explicitly tailored to account for their behaviour can be notable. One of the biggest contributors to the differences observed when scrutinising other NSPs is the lack of suitable models for spectral reduction either via non-linear or over-damped spectra that can capture the behaviour of such non-ductile frames with infills. This behaviour is characterised with a multilinear backbone with large loss of strength due to the formation of a non-ductile mechanism that occurs following infill panel collapse. This is evident following the comparisons conducted previously and illustrated in Figs. 13 and 14. A much better correlation with the actual NLTHA results in terms of vulnerability and risk was observed when using the proposed PB-Risk methodology.

While a conservative estimate may appeal to analysts, since a safety margin is implied, this may not be entirely adequate when utilising these results in a broader setting with possible financial implications in overestimating the losses attributed to a particular risk level. Future development of the proposed PB-Risk methodology will foresee the integration of the current findings (i.e. seismic demand parameters, annual rates of exceedance) with economic loss assessment using simplified concepts such as storey-loss functions (Shahnazaryan and O'Reilly 2021; Shahnazaryan et al. 2021, 2022; Papadopoulos et al. 2019) and indirect losses (Calvi et al. 2021) for a more thorough probabilistic assessment incorporating all relevant aspects of the PBEE framework.

6 Summary and conclusions

The accurate seismic risk assessment and evaluation of reinforced concrete (RC) structures with masonry infills remains an open challenge for practitioners and decision-makers due to their prevalence in the global built environment and complex behaviour. In risk-based analyses, accurate characterisation of infilled RC building performance based on code-based limit-state thresholds is paramount. Furthermore, non-linear time-history analyses (NLTHA) methods can be computationally expensive in terms of time and effort to allow widespread and codified implementation. Additionally, recent and upcoming technical standards for assessing existing structures improve on the shortcomings of existing guidelines characterising seismic risk via capacity-to-demand ratios as a deterministic manner of carrying out verifications. The adoption of loading-based quantities in governmental risk classification schemes has been shown to be somewhat limited in communicating actual seismic risk in existing buildings. To this end, this paper proposes a simplified pushover-based probabilistic methodology for the seismic risk evaluation of existing infilled RC building structures (PB-Risk). It integrates closed-form expressions for characterising seismic hazard and fragility estimates using a series of recently developed tools for infilled RC frames for risk-based applications. The aim was to provide an accurate methodology to quantify the seismic risk of the infilled RC typology and facilitate the needs of risk

modellers, ease the burden of computationally expensive procedures and address their limitations. Some of the main outcomes of this study are:

- A case study application on code-compliant and degrading (i.e., simulating non-compliant existing structures) SDOF systems highlighted the non-uniformity of loading-based quantities adopted in risk classification guidelines like Sismabonus in Italy or %NBS in New Zealand. Their difficulties in accurately and robustly conveying seismic risk for structures of different vibration period and lateral strength was illustrated, where equivalent actual risks can be found across different risk classes.
- A methodology was presented for the simplified pushover-based seismic risk assessment of non-ductile infilled RC frame buildings. The method relies on a (1) second-order power-law fit for the characterisation of seismic hazard; (2) a pushover-based response estimation tool for the fast evaluation of empirical strength-ductility relationships to quantify their seismic vulnerability; and (3) closed-form expressions to estimate mean annual frequency of limit-state exceedance for risk-based applications.
- The performance of the proposed PB-Risk methodology in accurately defining seismic vulnerability and risk was validated within a comparative case study application. The results highlighted the reliability and consistency of the proposed approach when compared to the results of detailed analysis on numerical models with hazard-consistent ground motions.
- Existing code and guideline methods to estimate seismic performance such as capacity spectrum method (CSM), N2 method, displacement coefficient method (DCM) and SPO2IDA were also critically evaluated. Their results either consistently underestimated the seismic intensity required to exceed a given limit state intensity or a large scatter was observed in the results when compared to non-linear time-history analyses. This was especially the case for the CSM, DCM and SPO2IDA and highlighted their inconsistency and general difficulty when applied to infilled RC frame buildings. The N2 method, when extended to infilled RC frames, performed relatively well but the proposed PB-Risk methodology was seen to offer several improvements in this respect.
- Regarding risk-based metrics, the estimates of existing NSPs exhibited similar conservativeness with an overestimation of seismic risk compared to the benchmark risk values from NTLHA. However, PB-Risk demonstrated consistent results and a higher correlation to the same benchmark values. While conservativeness is more appealing for carrying-out design and assessment studies where safety margins are necessary, accuracy and consistency are arguably more desirable within a broader financial loss assessment setting, which the proposed method has been shown to offer.

Data availability The building models used as part of this study are freely available on Github at: https://github.com/gerardjoreilly/Infilled-RC-Building-Database.

Code availability The code used for response estimation is freely available on Github at: https://github.com/gerardjoreilly/Infilled-RC-Building-Response-Estimation.

Declarations

Conflicts of interest The authors have no conflicts of interest to declare that are relevant to the content of this article.

References

Applied Technology Council (1996) ATC 40 seismic evaluation and retrofit of concrete buildings redwood city California. Seism Saf Comm 1996(1):334

Baker JW (2011) Conditional mean spectrum: tool for ground-motion selection. J Struct Eng 137(3):322–331. https://doi.org/10.1061/(asce)st.1943-541x.0000215

Baker JW (2015) Efficient analytical fragility function fitting using dynamic structural analysis. Earthq Spectra 31(1):579–599. https://doi.org/10.1193/021113EQS025M

Baltzopoulos G, Chioccarelli E, Iervolino I (2015) The displacement coefficient method in near-source conditions. Earthq Eng Struct Dynam 44(7):1015–1033. https://doi.org/10.1002/eqe.2497

Baltzopoulos G, Grella A, Iervolino I (2021) Seismic reliability implied by behavior-factor-based design. Earthq Eng Struct Dynam. https://doi.org/10.1002/eqe.3546

Basha SH, Kaushik HB (2016) Behavior and failure mechanisms of masonry-infilled RC frames (in low-rise buildings) subject to lateral loading. Eng Struct 111:233–245. https://doi.org/10.1016/j.engstruct.2015.12.034

Belliss CJ, Fox MJ, Sullivan T (2016) Exploring the probability of collapse of RC frame structures designed to current New Zealand Standards.In: 2016 NZSEE Conference, Christchurch, New Zealand

Bergami AV, Nuti C (2015) Experimental tests and global modeling of masonry infilled frames. Earthq Struct 9(2):281–303. https://doi.org/10.12989/eas.2015.9.2.281

Bradley BA (2010) A generalized conditional intensity measure approach and holistic ground-motion selection. Earthq Eng Struct Dynam 39(12):1321–1342. https://doi.org/10.1002/eqe.995

Calvi GM, O'Reilly GJ, Andreotti G (2021) Towards a practical loss-based design approach and procedure. Earthq Eng Struct Dyn 50(14):3741–3753. https://doi.org/10.1002/eqe.3530

Chenouda M, Ayoub A (2008) Inelastic displacement ratios of degrading systems. J Struct Eng 134(6):1030–1045. https://doi.org/10.1061/(ASCE)0733-9445(2008)134:6(1030)

CNR (2014) Istruzioni per la valutazione affidabilistica della sicurezza sismica di edifici esistenti

Cornell CA, Jalayer F, Hamburger RO, Foutch DA (2002) Probabilistic basis for 2000 SAC federal emergency management agency steel moment frame guidelines. J Struct Eng 128(4):526–533. https://doi.org/10.1061/(ASCE)0733-9445(2002)128:4(526)

Cosenza E, Del Vecchio C, Di Ludovico M, Dolce M, Moroni C, Prota A et al (2018) The Italian guidelines for seismic risk classification of constructions: technical principles and validation. Bull Earthq Eng 16(12):5905–5935. https://doi.org/10.1007/s10518-018-0431-8

Crowley H, Despotaki V, Rodrigues D, Silva V, Toma-Danila D, Riga E et al (2020) Exposure model for European seismic risk assessment. Earthq Spectra 36(1):252–273. https://doi.org/10.1177/8755293020919429

Dolšek M, Fajfar P (2004) Inelastic spectra for infilled reinforced concrete frames. Earthq Eng Struct Dyn 33(15):1395–1416. https://doi.org/10.1002/eqe.410

Dolšek M, Fajfar P (2008) The effect of masonry infills on the seismic response of a four-storey reinforced concrete frame-a deterministic assessment. Eng Struct 30(7):1991–2001. https://doi.org/10.1016/j.engstruct.2008.01.001

Douglas J, Ulrich T, Negulescu C (2013) Risk-targeted seismic design maps for mainland France. Nat Hazards 65(3):1999–2013. https://doi.org/10.1007/s11069-012-0460-6

Eads L, Miranda E, Lignos DG (2015) Average spectral acceleration as an intensity measure for collapse risk assessment. Earthq Eng Struct Dyn 44(12):2057–2073. https://doi.org/10.1002/eqe.2575

Fajfar P (2000) A nonlinear analysis method for performance-based seismic design. Earthq Spectra 16(3):573–592. https://doi.org/10.1193/1.1586128

Fajfar P, Gašperšič P (1996) The N2 method for the seismic damage analysis of RC buildings. Earthq Eng Struct Dyn 25(1):31–46. https://doi.org/10.1002/(SICI)1096-9845(199601)25:1%3c31::AID-EQE534%3e3.0.CO;2-V

Fajfar P, Marusic D, Perus I (2005) Torsional effects in the pushover-based seismic analysis of buildings. J Earthq Eng 9(6):831–854. https://doi.org/10.1080/13632460509350568

Fardis MN (2018) Capacity design: early history. Earthq Eng Struct Dynam 47(14):2887–2896. https://doi.org/10.1002/eqe.3110

Fardis MN, Calvi GM (1994) Effects of infills on the global response of reinforced concrete frames In: Proceedings on the 10th European conference on earthquake engineering, Vienna, Balkema, Rotterdam

Federal Emergency Management Agency (2000) Prestandard and commentary for the seismic rehabilitation of buildings Reports FEMA 356. Washington, DC

FEMA (2012) FEMA P58–1. Seismic performance assessment of buildings: methodology, vol 1, pp 58–1, Washington, DC

Ferner H (2018) A seismic building rating system–the New Zealand experience. In: 17th US-Japan-New Zealand workshop on the improvement of structural engineering and resilience, Queenstown, New Zealand

Freeman SA (1998). Development and use of capacity spectrum method. In: proceedings of the 6th US NCEE conference on earthquake engineering/EERI (Paper 269), 12

Gaetani d'Aragona M, Polese M, Prota A (2020) Stick-IT: a simplified model for rapid estimation of IDR and PFA for existing low-rise symmetric infilled RC building typologies. Eng Struct 223:111182. https://doi.org/10.1016/j.engstruct.2020.111182

Gentile R, Galasso C (2021) Simplicity versus accuracy trade-off in estimating seismic fragility of existing reinforced concrete buildings. Soil Dyn Earthq Eng 144:106678. https://doi.org/10.1016/j.soildyn.2021.106678

Gkimprixis A, Tubaldi E, Douglas J (2019) Comparison of methods to develop risk-targeted seismic design maps. Bull Earthq Eng 17(7):3727–3752. https://doi.org/10.1007/s10518-019-00629-w

Günay S, Mosalam KM (2013) PEER performance-based earthquake engineering methodology revisited. J Earthq Eng 17(6):829–858. https://doi.org/10.1080/13632469.2013.787377

Iervolino I, Giorgio M, Galasso C, Manfredi G (2010) Conditional hazard maps for secondary intensity measures. Bull Seismol Soc Am 100(6):3312–3319. https://doi.org/10.1785/0120090383

Iervolino I, Spillatura A, Bazzurro P (2018) Seismic reliability of code-conforming Italian buildings. J Earthq Eng 22(sup2):5–27. https://doi.org/10.1080/13632469.2018.1540372

Ioanna I, Borg R, Novelli V, Melo J, Alexander D, Kongar I, Verucci E, Cahill B, Rossetto T (2012) The 29th May Emilia Romagna Earthquake

Jalayer F, Cornell CA (2009) Alternative non-linear demand estimation methods for probability-based seismic assessments. Earthq Eng Struct Dyn 38(8):951–972. https://doi.org/10.1002/eqe.876

Kaatsiz K, Alici FS, Sucuoğlu H (2017) Generalized pushover analysis for torsionally coupled systems. In: 16th world conference on earthquake, Santiago, Chile

Kan CL, Chopra AK (1977) Effects of torsional coupling on earthquake forces in buildings. J Struct Div 103(4):805–819. https://doi.org/10.1061/JSDEAG.0004608

Kohrangi M, Bazzurro P, Vamvatsikos D, Spillatura A (2017) Conditional spectrum-based ground motion record selection using average spectral acceleration. Earthq Eng Struct Dyn 46(10):1667–1685. https://doi.org/10.1002/eqe.2876

Krawinkler H (1994) New trends in seismic design methodology. In: 10th European conference on earthquake engineering, Vienna, Austria

Landi L, Tardini A, Diotallevi PP (2016) A procedure for the displacement-based seismic assessment of infilled RC frames. J Earthq Eng 20(7):1077–1103. https://doi.org/10.1080/13632469.2015.1112324

Li Y, Yin Y, Ellingwood BR, Bulleit WM (2010) Uniform hazard versus uniform risk bases for performance-based earthquake engineering of light-frame wood construction. Earthq Eng Struct Dyn 39(11):1199–1217. https://doi.org/10.1002/eqe.989

Lin T, Haselton CB, Baker JW (2013) Conditional spectrum-based ground motion selection. Part I: hazard consistency for risk-based assessments. Earthq Eng Struct Dyn 42(12):1847–1865. https://doi.org/10.1002/eqe.2301

MBIE (2017) The seismic assessment of existing buildings, technical guidelines for engineering assessments

Milanesi RR, Morandi P, Hak S, Magenes G (2021) Experiment-based out-of-plane resistance of strong masonry infills for codified applications. Eng Struct 242:112525. https://doi.org/10.1016/j.engstruct.2021.112525

Ministero delle Infrastrutture e dei Trasporti. D.M del 17 Gennaio (2018) Aggiornamento delle Norme tecniche per le Costruzioni. Supplemento Ordinario Alla "Gazzetta Ufficiale,, n 42 Del 20 Febbraio 2018- Serie Generale ,1–198

Miranda E, Bertero VV (1994) Evaluation of strength reduction factors for earthquake-resistant design. Earthq Spectra 10(2):357–379. https://doi.org/10.1193/1.1585778

Morandi P, Hak S, Magenes G (2018) Performance-based interpretation of in-plane cyclic tests on RC frames with strong masonry infills. Eng Struct 156:503–521. https://doi.org/10.1016/j.engstruct.2017.11.058

Morandi P, Hak S, Milanesi RR, Magenes G (2022) In-plane/out-of-plane interaction of strong masonry infills: From cyclic tests to out-of-plane verifications. Earthq Eng Struct Dynam 51(3):648–672. https://doi.org/10.1002/eqe.3584

Morandi P, Hak S, Magenes G (2014) In-plane experimental response of strong masonry infills. In: 9th international masonry conference, Guimaraes, Portugal

Mori F, Mendicelli A, Moscatelli M, Romagnoli G, Peronace E, Naso G (2020) A new Vs30 map for Italy based on the seismic microzonation dataset. Eng Geol 275:105745. https://doi.org/10.1016/j.enggeo.2020.105745

Nafeh AMB, O'Reilly GJ, Monteiro R (2020) Simplified seismic assessment of infilled RC frame structures. Bull Earthq Eng 18(4):1579–1611. https://doi.org/10.1007/s10518-019-00758-2

Nafeh AM, O'Reilly GJ (2022) Unbiased simplified seismic fragility estimation of non-ductile infilled RC structures. Soil Dynam Earthq Eng 157:107253. https://doi.org/10.1016/j.soildyn.2022.107253

Nettis A, Gentile R, Raffaele D, Uva G, Galasso C (2021) Cloud capacity spectrum method: Accounting for record-to-record variability in fragility analysis using nonlinear static procedures. Soil Dynam Earthq Eng 150:106829. https://doi.org/10.1016/j.soildyn.2021.106829

O'Reilly GJ (2021a) Seismic intensity measures for risk assessment of bridges. Bull Earthq Eng. https://doi.org/10.1007/s10518-021-01114-z

O'Reilly GJ (2021b) Limitations of Sa(T 1) as an intensity measure when assessing non-ductile infilled RC frame structures. Bull Earthq Eng 19(6):2389–2417. https://doi.org/10.1007/s10518-021-01071-7

O'Reilly GJ, Nafeh AMB (2021a) Infilled-RC-building-response-estimation. GitHub Repos. https://doi.org/10.5281/zenodo.5082996

O'Reilly GJ, Nafeh AMB (2021b) Infilled-RC-building-database. GitHub Repos. https://doi.org/10.5281/zenodo.5082990

O'Reilly GJ (2016) Performance-based seismic assessment and retrofit of existing RC frame buildings in Italy, IUSS Pavia, vol 477. https://doi.org/10.13140/RG.2.2.32605.97761

Ozsarac V, Monteiro R, Calvi GM (2021) Probabilistic seismic assessment of reinforced concrete bridges using simulated records. Struct Infrastruct Eng. https://doi.org/10.1080/15732479.2021.1956551

Pagani M, Monelli D, Weatherill G, Danciu L, Crowley H, Silva V et al (2014) Openquake engine: an open hazard (and risk) software for the global earthquake model. Seismol Res Lett 85(2):692–702. https://doi.org/10.1785/0220130087

Papadopoulos AN, Vamvatsikos D, Kazantzi AK (2019) Development and application of FEMA P-58 compatible story loss functions. Earthq Spectra 35(1):95–112. https://doi.org/10.1193/102417EQS222M

Parisi F, Luca F De, Petruzzelli F, Risi R De, Chioccarelli E (2012) Field inspection after the May 20th and 29th 2012 Emilia-Romagna earthquakes. Rep Italian Network Earthquake Engineering University Laboratories

Petruzzelli F, Iervolino I (2021) NODE: a large-scale seismic risk prioritization tool for Italy based on nominal structural performance. Bull Earthq Eng 19(7):2763–2796. https://doi.org/10.1007/s10518-021-01093-1

Pinto P, Franchin P (2016) Probabilistic seismic assessment of existing buildings. In: Gardoni P, LaFave JM (eds) The CNR-DT212 Italian provisions. Springer, Cham. https://doi.org/10.1007/978-3-319-29713-2_7

Priestley MJN, Calvi GM, Kowalsky MJ (2007) Displacement based seismic design of structures. IUSS Press, Pavia

Qian J, Dong Y (2020) Multi-criteria decision making for seismic intensity measure selection considering uncertainty. Earthq Eng Struct Dyn 49(11):1095–1114. https://doi.org/10.1002/eqe.3280

Shahnazaryan D, O'Reilly GJ (2021) Integrating expected loss and collapse risk in performance-based seismic design of structures. Bull Earthq Eng 19(2):987–1025. https://doi.org/10.1007/s10518-020-01003-x

Shahnazaryan D, O'Reilly GJ, Monteiro R (2021) Story loss functions for seismic design and assessment: development of tools and application. Earthq Spectra 37(4):2813–2839. https://doi.org/10.1177/87552930211023523

Shahnazaryan D, O'Reilly GJ, Monteiro R (2022) On the seismic loss estimation of integrated performance-based designed buildings. Earthq Eng Struct Dyn 51(8):1794–1818. https://doi.org/10.1002/eqe.3638

Shi W, Lu X, Ye L (2012) Uniform-risk-targeted seismic design for collapse safety of building structures. Sci China Technol Sci 55(6):1481–1488. https://doi.org/10.1007/s11431-012-4808-7

Stucchi M, Meletti C, Montaldo V, Akinci A, Faccioli E, Gasperini P, Malagnini L, Valensise G (2004) Pericolosità sismica di riferimento per il territorio nazionale MPS04 [Data set]. Istituto Nazionale di Geofisica e Vulcanologia (INGV). https://doi.org/10.13127/sh/mps04/ag

European Standard (2003) Eurocode 8: design of structures for earthquake resistance—Part 1: General rules, seismic actions and rules for buildings. European Committee for Standardization

Ulrich T, Negulescu C, Douglas J (2014) Fragility curves for risk-targeted seismic design maps. Bull Earthq Eng 12(4):1479–1491. https://doi.org/10.1007/s10518-013-9572-y

Vamvatsikos D (2013) Derivation of new SAC/FEMA performance evaluation solutions with second-order hazard approximation. Earthq Eng Struct Dyn 42(8):1171–1188. https://doi.org/10.1002/eqe.2265

Vamvatsikos D, Cornell CA (2005) Direct estimation of seismic demand and capacity of multidegree-of-freedom systems through incremental dynamic analysis of single degree of freedom approximation. J Struct Eng 131(4):589–599. https://doi.org/10.1061/(asce)0733-9445(2005)131:4(589)

Vamvatsikos D, Cornell CA (2006) Direct estimation of the seismic demand and capacity of oscillators with multi-linear static pushovers through IDA. Earthq Eng Struct Dyn 35(9):1097–1117. https://doi.org/10.1002/eqe.573

Woessner J, Laurentiu D, Giardini D, Crowley H, Cotton F, Grünthal G et al (2015) The 2013 European seismic hazard model: key components and results. Bull Earthq Eng 13(12):3553–3596. https://doi.org/10.1007/s10518-015-9795-1

Zhai C, Kong J, Wang X, Chen Z (2016) Experimental and finite element analytical investigation of seismic behavior of full-scale masonry infilled rc frames. J Earthq Eng 20(7):1171–1198. https://doi.org/10.1080/13632469.2016.1138171